Appl Phys A
DOI 10.1007/s00339-008-5047-4

Applied Physics A
Materials Science & Processing

Modal resonant ultrasound spectroscopy for ferroelastics

Michal Landa · Petr Sedlák · Hanuš Seiner · Luděk Heller · Lucie Bicanová · Petr Šittner · Václav Novák

Received: 31 August 2007 / Accepted: 24 November 2008
© Springer-Verlag 2009

Abstract Recent experimental and theoretical improvements of resonant ultrasound spectroscopy (RUS) are summarized to investigate elastic constants of phases in shape memory alloys. The proposed inversion procedure, described in this work, is particularly suitable to reliable evaluation of the temperature dependence of elastic constants of low-symmetry ferroelastic materials which may be strongly elastically anisotropic and tend to exist in twinned forms. The method is applicable even for the evaluation of single-crystal elastic constants from RUS measurements on microtwinned crystals, since it involves a homogenization algorithm based on the macroscopic deformation response of the layered structure. This potentially allows performing meaningful acoustic studies on samples with a general submicron-size layered structure.

PACS 62 · 62.20.de · 62.20.fg · 62.25.Jk · 62.30.+d

M. Landa (✉) · P. Sedlák · H. Seiner · L. Heller · L. Bicanová
Institute of Thermomechanics, v.v.i., Academy of Sciences of the Czech Republic, Dolejškova 5, Prague 8, 182 00, Czech Republic
e-mail: ml@it.cas.cz
Fax: +420-28658-4695

P. Šittner · V. Novák
Institute of Physics, v.v.i., Academy of Sciences of the Czech Republic, Na Slovance 2, Prague 8, 182 21, Czech Republic

P. Sedlák · H. Seiner · L. Bicanová
Faculty of Nuclear Sciences and Physical Engineering, Czech Technical University in Prague, Trojanova 13, Prague 2, 120 00, Czech Republic

Published online: 13 January 2009

1 Introduction

Resonant ultrasound spectroscopy (RUS) is a well-known technique for investigation of elastic properties of solids based on the inversion of natural frequencies of free elastic vibrations of a small simply shaped specimen [1]. Comparing with pulse-echo ultrasonic methods, the main advantage of the RUS method is that elastic constants can be determined from a single measurement. For this reason, the method can be employed for measurements of temperature dependences of elastic constants, which are fundamental thermodynamic properties of solids and give essential information on the phase structure stability.

The RUS method has been successfully applied for characterization of composite materials. Elastic constants of dissimilar layers composed into isotropic laminates were determined by RUS technique using discrete-layer approximation for 3D vibration model, as may be found in [2], and a prediction of elastic properties of MCC composites with hexagonal symmetry by several phenomenological micromechanical models was utilized in [3]. The extension of variational formulas for evaluation of piezoelectric properties of layered structures was described in [4]. The RUS method also has a great potential in the field of mechanical spectroscopy and evaluation of internal friction in materials [5, 6]. A great importance of RUS methods was found in NDT and quality control techniques. For example, the RUS method involving Rayleigh mode resonance technique was applied to detect surface cracks on bearing ceramic balls [7]. Several experimental RUS techniques exploiting nonlinear phenomena have been recently developed [8, 9].

Standard analysis of resonances (RPR algorithm described in [1]) is based on a comparison of measured resonance frequencies with free-vibration calculation. This comparison requires reliable mode identification, which can be

significantly increased by characterizing eigenmodes of the vibration by laser interferometry measurements of displacement distribution patterns [10].

Elastic properties of strongly anisotropic single crystals of phase transforming materials, discussed widely in [11], complicate the use of the conventional RUS method with the standard RPR algorithm [12] because of the need to involve a large number of resonances. The extension of the RUS method, Modal RUS (MRUS), applicable to a general parallelepiped arbitrarily oriented specimen of strongly anisotropic crystals is briefly referred in [13, 14], where a novel optimization approach for the inversion is introduced, employing both resonance frequencies and the corresponding eigenmodes as inputs.

In this paper, we summarize recent experimental and theoretical improvements of resonant ultrasound spectroscopy for investigation of elastic constants of individual phases of SMA:

(i) A reliable vibration mode identification exploiting scanning laser interferometry measurement, which leads to a well-posed resonance inversion.
(ii) Estimation of accuracy in the evaluation of elastic constants or their combinations.
(iii) Stabilization of RUS inversion by phase velocity measurements (pulse-echo method).
(iv) A homogenization model based on the macroscopic deformation response of the layered structure, and its application to microtwinned crystals. This approach, more general than [5], may be found of particular importance to the analysis of elastic properties of ferroelastic solids and other intermetallics.

2 Fundamentals and extensions of RUS

2.1 Dynamic model for anisotropic parallelepiped vibration: forward problem of RUS

The forward problem of RUS lies in the evaluation of eigenfrequencies and eigenmodes of free vibrations of an elastic specimen. The resonance frequencies and eigenmodes of such can be sought by finding stationary points of the Lagrangian

$$\Lambda = \frac{1}{2}\int_V \left[\rho\omega^2 u_i^2(\mathbf{x}) - C_{ijkl}\frac{\partial u_i}{\partial x_j}(\mathbf{x})\frac{\partial u_k}{\partial x_l}(\mathbf{x})\right] \mathrm{d}V, \tag{1}$$

where V is the specimen's volume, C_{ijkl} is the tensor of elastic coefficients, $\mathbf{u}(\mathbf{x})$ is the displacement field, ρ is the mass density, and ω is the sought eigenfrequency.

In general, a solution of (1) may not have a closed-form, and this problem must be, thus, solved numerically, as it can be found in literature, e.g., [1], for many different shapes of either homogeneous or heterogeneous sample. If the specimen is homogeneous and has a simple shape, the Ritz method seems to be the most effective numerical procedure. In case of measuring single crystals of SMAs, rectangular shaped specimens are the most convenient, which allows us to combine, at the same time, the RUS technique with pulse-echo measurement (advantages of this will be discussed below). When rectangular sample transforms from austenite to a single-variant martensite, it changes its shape to a nonrectangular parallelepiped. For this reason, we develop, in the following paragraph, the eigenmodes computation by Ritz method for anisotropic, nonrectangular parallelepiped.

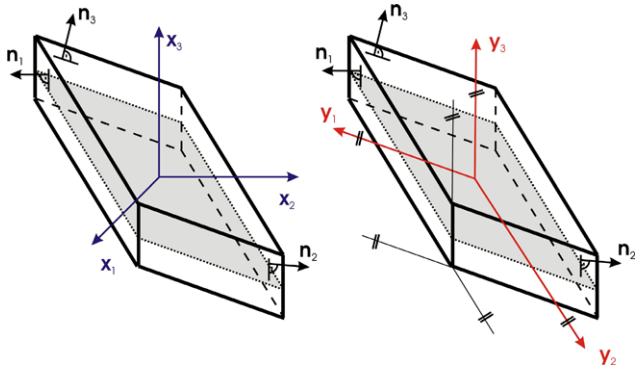

Fig. 1 Geometry of the parallelepiped and introduction of coordinate axes

Let us consider an anisotropic, nonrectangular parallelepiped in Fig. 1. In the Cartesian coordinate system $\mathbf{X} = \{\mathbf{x}_1, \mathbf{x}_2, \mathbf{x}_3\}$, let the anisotropic elasticity be described by the tensor C_{ijkl}. Geometry of a specimen is given by unit normals $\mathbf{n}_1, \mathbf{n}_2, \mathbf{n}_3$ to the parallelepiped's faces, and dimensions d_1, d_2, d_3 (measured in directions of the normals).

Now, consider linear transformation of vector coordinates in the $\mathbf{X}$ basis into coordinates in a new $\mathbf{Y}$ basis given by

$$(\mathbf{p})_\mathbf{Y} = \mathbf{B}(\mathbf{p})_\mathbf{X}, \tag{2}$$

where $\mathbf{B}$ is a regular matrix defined as

$$\mathbf{B} = \begin{pmatrix} (\mathbf{n}_1)_{x_1} & (\mathbf{n}_1)_{x_2} & (\mathbf{n}_1)_{x_3} \\ (\mathbf{n}_2)_{x_1} & (\mathbf{n}_2)_{x_2} & (\mathbf{n}_2)_{x_3} \\ (\mathbf{n}_3)_{x_1} & (\mathbf{n}_3)_{x_2} & (\mathbf{n}_3)_{x_3} \end{pmatrix}. \tag{3}$$

It is obvious that the base vectors $\{\mathbf{y}_1, \mathbf{y}_2, \mathbf{y}_3\}$ of $\mathbf{Y}$ are parallel to the parallelepiped's edges (thus, form a nonorthogonal coordinate system) and fulfil the normalization condition $(\mathbf{y}_i \cdot \mathbf{n}_i) = 1$ (no sum convention).

Applying the substitution (2) in the Lagrangian (1), we obtain

$$\Lambda = \frac{1}{2}\int_{-\frac{d_1}{2}}^{+\frac{d_1}{2}}\int_{-\frac{d_2}{2}}^{+\frac{d_2}{2}}\int_{-\frac{d_3}{2}}^{+\frac{d_3}{2}}\left[\frac{\rho}{\Im}\omega^2 u_i^2(\mathbf{y}) - T_{ijkl}\frac{\partial u_i}{\partial y_j}(\mathbf{y})\frac{\partial u_k}{\partial y_l}(\mathbf{y})\right]\mathrm{d}y_1\,\mathrm{d}y_2\,\mathrm{d}y_3, \tag{4}$$

where $\Im = \det \mathbf{B}$ is the Jacobian of the considered transformation, and

$$T_{ijkl} = \frac{1}{\Im}C_{ipko}B_{jp}B_{lo}. \tag{5}$$

The four-dimensional array T_{ijkl} relates the elasticity of the material (point property given by tensor C_{ipko}), with the sample geometry given by the product $B_{jp}B_{io.}$. For a mutual rotation of the geometry, T_{ijkl} does not follow the transformation rules for the fourth-order tensor but possesses major symmetry $T_{ijkl} = T_{klij}$. The advantage of using T_{ijkl} rather than a fully rotated tensor lies in a considerably faster evaluation of this array. This approach keeps the displacement vector $\mathbf{u}$ in the original coordinate system $\mathbf{X}$ (even if it is a function of the nonorthogonal coordinates $\mathbf{Y}$).

By this transformation, we obtained formally the same expression of Lagrangian as for the rectangular specimen which was already solved in literature, originally by [15], later by [1]. Following the paper [15], the Ritz method was applied by taking base functions in the form

$$\Psi_{abc} = P_a\left(\frac{2y_1}{d_1}\right)P_b\left(\frac{2y_2}{d_2}\right)P_c\left(\frac{2y_3}{d_3}\right),\quad a,b,c = 0,1,2,3,\ldots,\ a+b+c \le N, \tag{6}$$

where $P_n(y)$ is the normalized Legendre polynomial of degree n defined as

$$P_n(y) = \frac{\sqrt{(2n+1)/2}}{2^n n!}\left[\frac{d^n}{dy^n}\left(y^2-1\right)^n\right]. \tag{7}$$

In this basis, the solution is expanded as

$$u_i(\mathbf{y}) = \sum_{abc}\alpha_{[abc,i]}\Psi_{abc}(\mathbf{y}). \tag{8}$$

Condition for stationary points of the Lagrangian Λ leads to the symmetric eigenvalue problem

$$\left(\omega^2\mathbf{E}_{[abc,i],[def,j]} - \mathbf{\Gamma}_{[abc,i],[def,j]}\right)\alpha_{[abc,i]} = 0, \tag{9}$$

where

$$\mathbf{E}_{[abc,i],[def,j]} = \delta_{ij}\delta_{ad}\delta_{be}\delta_{cf}, \tag{10}$$

$$\mathbf{\Gamma}_{[abc,i],[def,j]} = \frac{\Im}{\rho}\frac{8}{d_1d_2d_3}T_{ijkl} \times \int_{-\frac{d_1}{2}}^{+\frac{d_1}{2}}\int_{-\frac{d_2}{2}}^{+\frac{d_2}{2}}\int_{-\frac{d_3}{2}}^{+\frac{d_3}{2}}\frac{\partial\Psi_{abc}}{\partial y_k}\frac{\partial\Psi_{def}}{\partial y_l}\,\mathrm{d}y_1\,\mathrm{d}y_2\,\mathrm{d}y_3. \tag{11}$$

For effective computation of the matrix $\mathbf{\Gamma}$, the integrals D_{mn} and N_{mn} were computed in advance, using symbolic algebra (Symbolic Math Toolbox™):

$$D_{mn} = \int_{-1}^{1}\frac{\mathrm{d}P_m(x)}{\mathrm{d}x}\frac{\mathrm{d}P_n(x)}{\mathrm{d}x}\,\mathrm{d}x, \tag{12}$$

$$N_{mn} = \int_{-1}^{1}\frac{\mathrm{d}P_m(x)}{\mathrm{d}x}P_n(x)\,\mathrm{d}x. \tag{13}$$

The Cholesky algorithm, implemented in the standard Matlab$^{\mathrm{R}}$ routine `eig.m`, was used for determination of both the eigenfrequencies and eigenvectors of (9).

Note that $\mathbf{E}$ is the unity matrix. Some authors [1, 16] use the base functions of the type $x^r y^p z^q$ for modeling more general shapes of solids. In that case, $\mathbf{E}$ is a full matrix, and (9) represents a generalized eigenvalue problem.

The accuracy of the solution of problem (1) by the Ritz method depends on maximum degree of the Legendre polynomial N taken in expression (6). By increasing N, precision is increasing, but on the other hand, computation time for solving (9) increases dramatically, since the dimension of the matrix $\mathbf{\Gamma}$ is given by

$$\mathrm{rank}(\mathbf{\Gamma}) = (N+1)(N+2)(N+3)/2. \tag{14}$$

Arbitrary material symmetry and material coordinate system orientation is assumed in the present computation. In this general case, the inversion symmetry is the only common symmetry element of both the homogeneous parallelepiped and elastic constant matrix. According to [17], one can separate symmetric and antisymmetric base functions Ψ_{abc} (symmetric and antisymmetric Ψ_{abc} may be distinguished by whether $a+b+c$ is even or odd) and split the matrix $\mathbf{\Gamma}$ into two blocks. This decomposition of $\mathbf{\Gamma}$ considerably reduces computation time.

It is worth mentioning here the linear dependence of the matrix $\mathbf{\Gamma}$ on elastic constants C_{ijkl}, which comes directly from its definition (11). For the set of independent elastic constants C_k, the matrices $\partial\mathbf{\Gamma}/\partial C_k$ depend only on geometry, density N, and symmetry of the sample and can be evaluated a priori without specifying C_k. Consequently, the matrix $\mathbf{\Gamma}$ can be completed as

$$\mathbf{\Gamma} = \frac{\partial\mathbf{\Gamma}}{\partial C_k}C_k. \tag{15}$$

This property dramatically reduces time for iterative completion of $\mathbf{\Gamma}$ for a different set of C_k.

From (8) and (9) one can easily establish the surface distribution of the displacement field and consequently the displacement in the direction of face normal for each mode. Thus, for the face with normal $\mathbf{n}_1$, one obtains

$$v(y_2, y_3) = \sum_i \left((\mathbf{n}_1)_{x_i} \sum_{abc} \alpha_{[abc,i]} P_a(1) P_b\left(\frac{2y_2}{d_2}\right) P_c\left(\frac{2y_3}{d_3}\right)\right), \tag{16}$$

where $y_2 \in \langle -\frac{d_2}{2}, \frac{d_2}{2}\rangle$ and $y_3 \in \langle -\frac{d_3}{2}, \frac{d_3}{2}\rangle$ represent edge coordinates (analogically for $\mathbf{n}_2$ and $\mathbf{n}_3$).

2.2 Evaluation of elastic constants: inversion procedure

To evaluate the elastic constants, one must first solve the forward problem of calculating the natural frequencies from the elastic constants and then apply a nonlinear inversion procedure to find the required elastic constants from the measured natural frequencies. This means, in general, finding the optimal set of constants C_k minimizing the error function

$$F(C_k) = \sum_p \left(f_p^{\text{cal}}(C_k) - f_p^{\text{exp}}\right)^2, \tag{17}$$

where f_p^{cal} and f_p^{exp} are the corresponding calculated and measured frequencies of the pth measured mode.

The inversion procedure brings two fundamental problems. First of them is the correct assignment of experimental and calculated modes, the second is the determination of accuracies of different constants or their combinations obtained from this inversion.

An incorrect assignment of experimental and calculated modes is a source of many errors in classical RUS method, where the resonance response is detected at a single point of the sample. In this approach, simple ordering of calculated and measured frequencies is performed to associate corresponding modes. In both cases, either when one has an inaccurate estimation of constants C_k, or if some resonance is missed during measurements, the incorrectness appears. To avoid this uncertainty, normal displacements of the vibrating specimen surface are measured by scanning Laser–Doppler interferometry [13]. By obtaining this additional information about the shape of different eigenmodes, one can identify resonance modes and correctly associate the computed and measured frequencies. In the following text, the way in which this information is implemented to the inversion is described. Note that eigenmodes form a system of orthogonal vectors, but their surface projections do not. Hence, one should be aware of that identical projections may belong to different modes.

By the RUS method, the elastic coefficients can be identified with a large variation in accuracy. The question how to determine which coefficients can be evaluated precisely from the resonant spectra and which not, plays an improtant role, in particular, in strongly anisotropic materials. that there exist some combinations of elastic constants on which resonance frequencies sensitively depend (see example for cubic symmetry, where δf depends mainly on $\delta C'$ and δC_{44}). These combinations can be obtained by the following procedure:

Let $\boldsymbol{\alpha}_{1,2,\ldots,p}$ be the eigenvectors corresponding to measured eigenfrequencies $f^{\text{exp}}_{1,2,\ldots,p} = \omega^{\text{exp}}_{1,2,\ldots,p}/2\pi$. The derivative of the frequency f_j^{exp} with respect to the constant C_k can be expressed as (using a formula from perturbation theory)

$$\frac{\partial f_j^{\text{exp}}}{\partial C_k} = \frac{\boldsymbol{\alpha}_j^T \frac{\partial \boldsymbol{\Gamma}}{\partial C_k} \boldsymbol{\alpha}_j}{8\pi^2 \cdot f_j^{\text{exp}}}. \tag{18}$$

The rate of sensitivity of the measured spectrum to the particular elastic coefficient C_k can be taken as the sum of squares of such derivatives over the whole measured spectrum, i.e.,

$$\sum_{j=1..p} \left(\frac{\partial f_j^{\text{exp}}}{\partial C_k}\right)^2 = \sum_{j=1..p} \left(\frac{\boldsymbol{\alpha}_j^T \frac{\partial \boldsymbol{\Gamma}}{\partial C_k} \boldsymbol{\alpha}_j}{8\pi^2 \cdot f_j^{\text{exp}}}\right)^2. \tag{19}$$

The sensitivities analogical to (19), but with respect to linear combinations C_l^*, related to the original set of elastic coefficients C_k by the linear equations

$$C_k = \beta_{kl} C_l^*, \tag{20}$$

may be expressed as

$$S_l^2 = \sum_{j=1..p} \left(\frac{\partial f_j^{\text{exp}}}{\partial C_l^*}\right)^2 = \sum_{j=1..p} \left(\beta_{kl} \frac{\partial f_j^{\text{exp}}}{\partial C_k}\right)^2 = [\,\beta_{1l} \quad \ldots \quad \beta_{ql}\,]\mathbf{G}^T\mathbf{G} \begin{bmatrix} \beta_{1l} \\ \ldots \\ \beta_{ql} \end{bmatrix}, \tag{21}$$

where

$$\mathbf{G} = \begin{bmatrix} \frac{\partial f_1^{\text{exp}}}{\partial C_1} & \ldots & \frac{\partial f_1^{\text{exp}}}{\partial C_q} \\ \ldots & \ldots & \ldots \\ \frac{\partial f_p^{\text{exp}}}{\partial C_1} & \ldots & \frac{\partial f_p^{\text{exp}}}{\partial C_q} \end{bmatrix}. \tag{22}$$

The matrix $\mathbf{G}^T\mathbf{G}$ is symmetric, and its eigenvectors can be, thus, chosen to form an orthogonal normalized system. By sorting its eigenvalues in decreasing order and choosing $[\beta_{1l} \ \ldots \ \beta_{ql}]$ to be the lth eigenvector, the constants C_l^* are related to the original constants C_k by an orthogonal transformation, which orders the linear combinations C_1^* from the best determinable one to the one most difficult to obtain.

2.3 Architecture of inversion procedure

The used inversion procedure consisted of following steps:

(1) We consider a parallelepiped sample with given material symmetry, density ρ, and shape defined by face unit normals $\mathbf{n}_1, \mathbf{n}_2$, and $\mathbf{n}_3$ and distances of parallel faces d_1, d_2, d_3.

(2) We compute the matrices $\partial\mathbf{\Gamma}/\partial C_k$ (C_k is the set of independent elastic constants) by formula (11) setting $C_k = 1$ and $C_j = 0$ for all $j \neq k$. The maximal degree of the Legendre polynomial N should reflect the number of fitted resonances.

(3) We take a first estimation of the constants $C_k^{(0)}$, complete the matrix $\mathbf{\Gamma}$ using (15), and calculate its eigenvalues and eigenvectors.

(4) Using formula (16), we compute surface distributions of displacement corresponding to each mode and, using comparison of computed and experimentally measured distributions, we try to associate measured and computed spectra.

(5) We compute the matrix $\mathbf{G}^T\mathbf{G}$ with frequencies $f_j^{\exp}$ and the associated eigenvectors $\boldsymbol{\alpha}_j^{\mathrm{as}}$ and determine the linear combinations C_k^*. (The eigenvectors $\boldsymbol{\alpha}_j^{\mathrm{as}}$ do not exactly equal the experimental eigenvector, and thus the derivatives $\partial f_j^{\exp}/\partial C_k$ obtained from (18) are only approximate.)

(6) We minimize the error function

$$F\left(C_k^*\right) = \sum_{p\in\mathrm{assoc.}} \left(f_p^{\mathrm{cal}}\left(C_k^*\right) - f_p^{\exp}\right)^2. \tag{23}$$

The modes are associated such that the calculated frequency $f_p^{\mathrm{cal}}(C_k^*)$ always corresponds to the eigenvector $\boldsymbol{\alpha}$ which fulfils the condition

$$\left|\boldsymbol{\alpha}_p^{\mathrm{as}}.\boldsymbol{\alpha}\right| = \max_j\left(\left|\boldsymbol{\alpha}_p^{\mathrm{as}}.\boldsymbol{\alpha}_j\right|\right), \tag{24}$$

where $\boldsymbol{\alpha}_p^{\mathrm{as}}$ is the associated eigenvector to the frequency $f_p^{\exp}$ from Step 4, and $\boldsymbol{\alpha}_j$ are eigenvectors of $\mathbf{\Gamma}(C_j(C_k^*))$. The nonassociated modes were not taken into account in (23).

The minimization is performed by a gradient (Levenberg–Marquardt) method, which provides fast and straightforward convergence. The efficiency of the inverse determination of the elastic coefficients was improved by deriving the analytical expression of the gradient and the Hessian of the error function using formulae from perturbation theory

$$\frac{\partial\omega_j^2}{\partial C_k^*} = \boldsymbol{\alpha}_j^T\frac{\partial\mathbf{\Gamma}}{\partial C_k^*}\boldsymbol{\alpha}_j, \tag{25}$$

$$\frac{\partial^2\omega_j^2}{\partial C_k^*\partial C_l^*} = \boldsymbol{\alpha}_j^T\frac{\partial\mathbf{\Gamma}}{\partial C_k^*}\frac{\partial\boldsymbol{\alpha}_j}{\partial C_l^*} + \left(\frac{\partial\boldsymbol{\alpha}_j}{\partial C_l^*}\right)^T\frac{\partial\mathbf{\Gamma}}{\partial C_k^*}\boldsymbol{\alpha}_j, \tag{26}$$

where

$$\frac{\partial\boldsymbol{\alpha}_j}{\partial C_l^*} = \sum_{\substack{i\\ \omega_i\neq\omega_j}}\frac{\boldsymbol{\alpha}_i^T\frac{\partial\mathbf{\Gamma}}{\partial C_l^*}\boldsymbol{\alpha}_j}{\omega_j^2-\omega_i^2}\boldsymbol{\alpha}_i. \tag{27}$$

The refinement of the constants are sequential; we firstly release only C_1^* and then add subsequent constants one by one.

(7) Accuracy of the evaluated constants C_j^* is estimated from the expression

$$\kappa_j = \sqrt{\frac{\sum_{p\in\mathrm{assoc.}}(f_p^{\mathrm{cal}}-f_p^{\exp})^2}{\sum_{p\in\mathrm{assoc.}}(\frac{\partial f_p^{\mathrm{cal}}}{\partial C_j^*})^2}}. \tag{28}$$

The constants C_j^* with low value of κ_j are accepted, the rest is replaced by the first estimation, and $C_j^{(1)}$ are reversibly computed from (20). Then we return back to Step 3 with new constants $C_j^{(1)}$ and repeat this process until we match all the measured resonances and fit their frequencies.

This reformulated inversion with parameters C_l^* sorted by their sensitivities S_l (rather than the original constants C_k) enables us to perform the optimization gradually (firstly for C_1^*, other fixed, secondly for C_1^* and C_2^*, etc.) up to a chosen sensitivity level. Hence, the inverse procedure is more robust than the classical method optimizing all original constants C_k together. This minimization approach starts with the initial guess $C_k^{(0)}$, which can be chosen ad hoc or obtained from preliminary pulse-echo measurements. If the guess is far from the exact values of elastic constants, only some first modes can be associated at the first step of the procedure. In the next step (next approximation of C_k), the mode association may be completed.

3 Example: RUS measurement on CuAlNi single crystal

As mentioned above, the RUS method is capable to determine the elastic constants of the individual phases from the measurements on one specimen. The following example demonstrates sensitivity of this method on a CuAlNi single crystal. It utilizes a hysteresis of transformation temperatures of B2 austenite and 2H martensite with orthorhombic symmetry, enabling the existence of both phases at room temperature.

The parallelepiped of the austenite was cut from a single crystal prepared by the Bridgeman method (dimensions $5.11 \times 6.16 \times 5.22$ mm, orientations [0.53 −0.80 −0.26], [0.81 0.58 −0.07], [0.21 −0.15 0.96]).

The RUS measurement on austenite was performed in the frequency range 0.1–0.6 MHz, and 65 identified modes were

Table 1 Coefficients of linear combinations C_l^* sorted by sensitivities S_l

l	(a) austenite phase			S_l
	$\beta_{l[11]}$	$\beta_{l[12]}$	$\beta_{l[44]}$	[kHz/GPa]
1	0.70970	−0.70141	0.06575	69.51
2	0.01024	0.10359	0.99456	2.80
3	0.70442	0.70517	−0.08070	0.20

l	(b) martensite phase									S_l
	$\beta_{l[11]}$	$\beta_{l[22]}$	$\beta_{l[33]}$	$\beta_{l[44]}$	$\beta_{l[55]}$	$\beta_{l[66]}$	$\beta_{l[23]}$	$\beta_{l[13]}$	$\beta_{l[12]}$	[kHz/GPa]
1	0.262	0.397	0.033	0.114	0.584	0.129	−0.134	0.076	−0.614	27.0
2	−0.187	−0.288	0.017	0.076	0.795	0.008	0.081	−0.092	0.477	11.1
3	0.003	−0.000	0.075	0.582	−0.150	0.780	−0.014	−0.083	0.128	3.6
4	−0.075	0.038	0.075	0.769	−0.054	−0.591	−0.196	0.052	0.013	2.8
5	0.273	−0.149	−0.143	0.179	−0.007	−0.125	0.748	−0.478	−0.212	1.7
6	0.153	0.148	0.568	−0.131	−0.026	−0.062	−0.315	−0.704	0.111	1.7
7	0.576	−0.717	0.206	0.011	−0.003	0.008	−0.216	0.214	−0.132	0.6
8	0.674	0.385	−0.323	0.008	0.001	−0.057	−0.044	0.074	0.530	0.2
9	0.072	0.221	0.704	−0.008	−0.004	−0.031	0.476	0.445	0.150	0.1

taken into account for the sensitivity analysis. Results are scheduled in Table 1a, where the coefficients of linear combination $C_l^* = \beta_{l[K]} C_{[K]}$, $l = 1, 2, 3$ and $[K] = 11, 12, 44$, are sorted by sensitivity S_l values in descending order. Sensitivity greater than 1.0 kHz/GPa is marked by red (dark grey), and values of $\beta_{l[K]} > 0.2$ are highlighted by magenta background (light grey).

The combinations C_k^* are numerically near the following quantities:

$$C_1^* \approx (C_{11} - C_{12})/\sqrt{2} = C'/\sqrt{2},$$

$$C_2^* \approx C_{44}, \qquad C_3^* \approx (C_{11} + C_{12})/\sqrt{2}.$$

Hence, the RUS results are very sensitive to C' and partially also to C_{44}, but reliable determination of the C_3^* is close to impossible. The resulting constants are:

$$C_1^* = (18.11 \pm 0.14)\ \text{GPa}, \qquad C_2^* = (108.38 \pm 2.14)\ \text{GPa},$$

$$C_3^* = (169.46 \pm 34.94)\ \text{GPa}.$$

A single-variant martensite crystal (nonrectangular 5.14 × 5.92 × 5.39 mm parallelepiped with face normals [−0.71; 0.58; −0.37], [0.32; 0.84; 0.42], [0.55; 0.23; −0.80]) was obtained from the austenite specimen by applying a sequence of compressions [11]. RUS measurement was performed in the frequency range 0.1–0.8 MHz, and 70 resonances were taken into account. The resulting weights of linear combination $\beta_{l[K]}$, $[K] = 11, 22, 33, 44, 55, 66, 23, 13, 12$ and $l = 1, 2, \ldots, 9$, are shown in Table 1b with the same sense of marking. The measurement exhibits low sensitivity to combinations C_7^*, C_8^*, and C_9^*. The original elastic constants C_k are widely distributed in the combinations. In this example, the constants C_{33}, C_{23}, and C_{13} are expected to be worse determined from the given frequency band. Even if the presented mode identification and introducing of eigenvectors into the optimization algorithm improve the RUS evaluation procedure and enable the extension of the range of analyzed spectra, there are still high frequency limits (∼100 resonances) given by the precision of calculation and possible overlapping of resonances. This upper limit of the frequency band also depends on the quality of resonances, which can be closely related to the quality of crystals.

4 Stabilization of the inverse procedure by the phase velocities

From the example described above, we can conclude that the reason why some of the linear combinations of the elastic coefficients cannot be accurately determined from the RUS measurements might be sought in that these combinations are somehow related to the fastest modes of elastic wave propagation in the considered material, which, due to the long wavelength, correspond only to minor part of the measured spectrum. Such an assumption can be validated by evaluating the sensitivity of phase velocity magnitudes in directions of the parallelepiped's face normals to the linear combinations C^*, see [14] for details. The low sensitive combinations are closely related to the phase velocities of quasi-longitudinal elastic waves in directions of normals to the parallelepipeds faces. The whole inversion

procedure may be stabilized by involving the results of additional acoustic velocity measurements (by means of, e.g., pulse-echo methods). Such a hybrid procedure gives some solution of the stabilization problem. Vice versa, this approach shows that the pulse-echo method itself cannot be used for reliable determination of those combinations of elastic coefficients which are closely related to the first resonant frequencies and can be, thus, reliably obtained from RUS measurements.

5 Temperature dependencies of elastic constants

The main importance of the RUS method for characterization of ferroelastics stems in reliability of determination of temperature dependences of elastic constants in a vicinity of the transition temperatures.

Reliable identification of the eigenmodes enables us to observe the temperature evolution of one individual mode. Via the formula

$$\frac{\mathrm{d}f_j}{\mathrm{d}T} = \frac{\boldsymbol{\alpha}_j^T \frac{\mathrm{d}\boldsymbol{\Gamma}}{\mathrm{d}T}\boldsymbol{\alpha}_j}{8\pi^2 \cdot f_j} \approx \sum_k \frac{\boldsymbol{\alpha}_j^T \frac{\partial \boldsymbol{\Gamma}}{\partial C_k}\boldsymbol{\alpha}_j}{8\pi^2 \cdot f_j} \frac{\mathrm{d}C_k}{\mathrm{d}T}, \tag{29}$$

similar to (18), we can relate temperature changes of elastic constants with temperature shifts of frequencies. In (29) we neglect change of matrix $\boldsymbol{\Gamma}$ due to thermal expansion, considering that

$$\frac{(\frac{\mathrm{d}C_k}{C_k})}{\mathrm{d}T} \gg \alpha, \tag{30}$$

where α is the coefficient of thermal expansion (a cubic crystal is assumed for simplicity without loss of general sense of the condition).

Expression (29) represents a system of linear equations for $\mathrm{d}C_k/\mathrm{d}T$, which can be solved, e.g., by simple least square method. It is worth noting that we are able to determine the temperature derivatives with a similar relative accuracy as for C_k, although the changes $\mathrm{d}C_k$ could be much smaller then the error in C_k.

6 Example: Temperature dependences of elastic constants of CoAlNi

The following example demonstrates the stabilization procedure and temperature measurement. It was performed on a parallelepiped specimen ($3.27 \times 3.89 \times 4.50$ mm with orientation [0.80 0.59 −0.08], [−0.11 −0.01 −0.99], [−0.58 0.81 0.08]) of austenite single crystal of CoAlNi (33.56 wt.% Ni, 26.83 wt.% Al). The cubic constant C' was determined from the first eight modes (only C_1^* was optimized):

$$C' = (5.33 \pm 0.22)\ \text{GPa} \quad \text{at } 11.4^\circ\text{C}, \quad \text{and}$$
$$(5.48 \pm 0.21)\ \text{GPa} \quad \text{at } 27^\circ\text{C}.$$

The error range was obtained by (28).

Remaining constants were determined by the hybrid method taking into account also quasilongitudinal and quasitransverse phase velocities measured by pulse-echo technique in the surface normal directions at RT (28°C):

$$C_{11} = 165.6\ \text{GPa}, \qquad C_{12} = 154.3\ \text{GPa},$$
$$C_{44} = 119.6\ \text{GPa}$$

with the accuracy better than 0.3%. Note that anisotropy factor A is about 22.

Frequency shifts of first eight vibration modes with temperature were taken into account for determination of $\mathrm{d}C'/\mathrm{d}T$ in three temperature intervals. The results were:

$$\mathrm{d}C'/\mathrm{d}T = (0.01226 \pm 0.00049)\ \text{GPa/K}$$
from 27.0 to 40.5°C,
$$\mathrm{d}C'/\mathrm{d}T = (0.01145 \pm 0.00026)\ \text{GPa/K}$$
from 11.4 to 27.0°C,
$$\mathrm{d}C'/\mathrm{d}T = (0.01078 \pm 0.00058)\ \text{GPa/K}$$
from −4.1 to 11.4°C.

The listed errors of $\mathrm{d}C'/\mathrm{d}T$ are given by 3σ interval of confidence of least square method.

7 Analysis of the twinned crystals

As the above described generalization enables the RUS method to be applied for an arbitrary parallelepiped, with no limitations to the class and orientation of the anisotropy, there is no reason to restrict the RUS investigation to single variants of martensite only. For some shape-memory alloys, or for specific orientation of the specimen, preparation of a pure single variant of martensite can encounter serious technical difficulties. In that case, if the elastic coefficients of the pure martensite require to be determined, the RUS measurement can be applied to an ordered mixture of martensitic variants, called *martensitic microstructure*. From determined effective elastic properties of such microstructured specimen and from known geometrical parameters of the microstructure, the elastic coefficients of the single variant can be evaluated.

7.1 Geometry and elastic properties of the twinned structure

Two assumptions must be done for the microstructured specimen to be suitable for such RUS investigation:

- The microstructure must be *fine*, i.e., a characteristic dimension of layered microstructure must be incomparably smaller than the specimen size.
- The microstructure must be *homogeneous*, i.e., the geometrical parameters and the composition of the microstructure should not alter in different regions of the specimen.

In Fig. 2a, a microstructure satisfying both these conditions is presented, whereas Fig. 2b shows an example of a fine but inhomogeneous microstructure.

With these two conditions fulfilled, the microstructured specimen can be treated as a homogeneous anisotropic material with elastic properties uniquely determined by the microstructure geometry and elastic properties of its particular components, martensitic variants.

Although the below described algorithms for evaluation and experimental determination of effective elastic properties of the microstructured body can be applied for any fine and homogeneous martensitic microstructure, it is natural to deal with the simplest and most frequently observed type of the *twinned structure*. Such structure is also called *a simple twin* or *the first-order laminate*, to be distinguished from the microstructure consisting of the crossing twins or fractal-like twins-within-twins structures. Hence, the supposed structure consists of a system of thin parallel laminae of two different variants of martensite with alternate thickness such that the resultant volume fraction of each variant is a constant.

7.2 Mutual orientation of variants in a twinned region

Let us consider a twinned structure consisting of two variants martensite denoted A and B, and let these variants

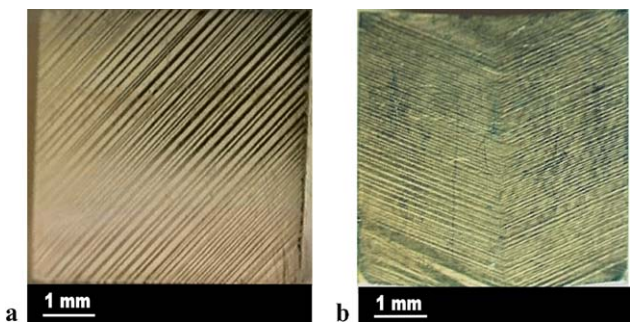

Fig. 2 Illustrative examples of twin structures (CuAlNi) over sample: (**a**) a simple twin laminate structure; (**b**) a fine but inhomogeneous microstructure (a macrotwin of two twinned regions)

are described by *Bain tensors* U^A and U^B. The Bain tensors determine the *transformation strain* between the parent austenitic phase and the particular variants martensite and are, thus, related via the rotation matrix Q^{AB} as follows:

$$U^A = \left(Q^{AB}\right)^T U^B Q^{AB}. \tag{31}$$

Similarly, the elastic properties of these two variants, each in its natural cartesian axes given by the basal lattice vectors, can be recalculated from each other by using the rule for rotation of tensor quantities,

$$C^A_{ijkl} = C^B_{mnpo} Q^{AB}_{im} Q^{AB}_{jn} Q^{AB}_{kp} Q^{AB}_{lo}. \tag{32}$$

To form a twin, the variants A and B must fulfill the compatibility condition

$$U^A - RU^B = \mathbf{a} \otimes \mathbf{n}, \tag{33}$$

where R is a matrix of mutual rotation of the variants in the twinning system, $\mathbf{n}$ is the orientation of the twinning plane (planar boundary between each two laminas) and $\mathbf{a}$ is a *shearing vector*, which does not have any direct geometrical interpretation in the twinned structure, but its existence itself ensures the existence of the A–B twinning system. The rotation matrix R enables the elastic properties of variant B in the twinning system to be expressed in the coordinate system of variant A, using the relation

$$C^{\tilde{B}}_{ijkl} = C^B_{mnpo} R_{im} R_{jn} R_{kp} R_{lo}. \tag{34}$$

7.3 Effective elastic coefficients evaluation

We will consider an infinitesimal microstructured volume $\mathrm{d}V$ including a sufficiently large number of parallel laminas of variants A and B such that $\mathrm{d}V$ can be considered as homogeneous. Let λ be the volume fraction of variant B, i.e., the variant A occupies the volume $(1-\lambda)\,\mathrm{d}V$ and variant B volume $\lambda\,\mathrm{d}V$. We assume that for each homogeneous small strain ε_{ij} of volume $\mathrm{d}V$, all lamina of each variant are deformed homogeneously with strains ε^A_{ij} and ε^B_{ij}, respectively, such that the condition

$$\left((1-\lambda)\varepsilon^A_{ij} + \lambda\varepsilon^B_{ij}\right) = \varepsilon_{ij} \tag{35}$$

is satisfied. Since each of the strain tensors has six independent components, (35) brings six linear conditions on 12 unknown components of ε^A_{ij} and ε^B_{ij}. The remaining six equations can be obtained from additional requirements at the twinning boundaries inside $\mathrm{d}V$.

These are the *stress equilibrium conditions*

$$\left(C^A_{ijkl}\varepsilon^A_{kl} - C^{\tilde{B}}_{ijkl}\varepsilon^B_{kl}\right)n_j = 0 \tag{36}$$

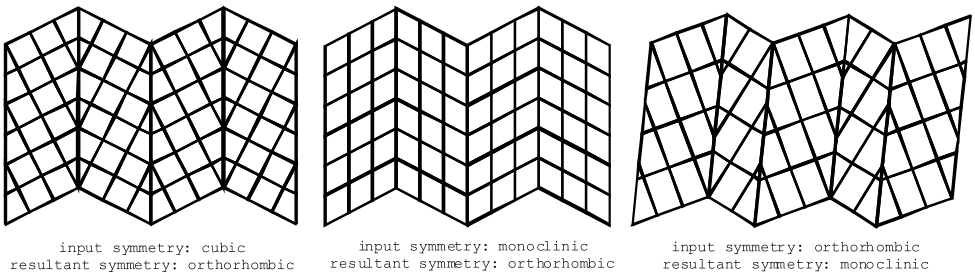

Fig. 3 Examples of input and resultant symmetries of twinned structures

and the conditions of *strain field compatibility*

$$\begin{aligned}&\left(\varepsilon_{ij}^{A}-\varepsilon_{ij}^{B}\right)v_i v_j=0,\qquad \left(\varepsilon_{ij}^{A}-\varepsilon_{ij}^{B}\right)w_i w_j=0,\quad \text{and}\\&\left(\varepsilon_{ij}^{A}-\varepsilon_{ij}^{B}\right)(w_i v_j+v_i w_j)=0,\end{aligned}\tag{37}$$

where **w** and **v** are two independent unit vectors lying in the twinning plane.

Equations (35)–(37) deliver for each given homogeneous strain ε_{ij} all independent components of strains ε_{ij}^{A} and ε_{ij}^{B}. The effective stored elastic energy density corresponding to such homogeneous strain can be written as the weighted average of stored elastic energy densities in particular variants, i.e.,

$$f(\varepsilon_{ij})=(1-\lambda)C_{ijkl}^{A}\varepsilon_{ij}^{A}\varepsilon_{kl}^{A}+\lambda C_{ijkl}^{\tilde{B}}\varepsilon_{ij}^{B}\varepsilon_{kl}^{B}.\tag{38}$$

However, this energy can also be expressed by the effective elastic coefficients as

$$f(\varepsilon_{ij})=C_{ijkl}\varepsilon_{ij}\varepsilon_{kl},\tag{39}$$

which is a linear combination of all C_{ijkl} components. So it is sufficient to take 21 strains ε_{ij} such that the fourth-rank tensors $\varepsilon_{ij}\varepsilon_{kl}$ are linearly independent to reformulate (38) and (39) to a linear system for unknown coefficients C_{ijkl}, where the particular strains ε_{ij}^{A} and ε_{ij}^{B} are, for each ε_{ij}, evaluated via (35)–(37). The strains ε_{ij} can be chosen in many different ways. We used all symmetric permutations of matrices

$$\begin{aligned}&\mathcal{E}_1=\begin{pmatrix}1&0&0\\0&0&0\\0&0&0\end{pmatrix},\qquad \mathcal{E}_2=\begin{pmatrix}0&1&0\\1&0&0\\0&0&0\end{pmatrix},\\&\mathcal{E}_3=\begin{pmatrix}1&1&0\\1&0&0\\0&0&0\end{pmatrix},\quad \text{and}\quad \mathcal{E}_4=\begin{pmatrix}0&1&1\\1&0&0\\1&0&0\end{pmatrix},\end{aligned}\tag{40}$$

which gives exactly 21 strains with independent $\varepsilon_{ij}\varepsilon_{kl}$ tensors.

The 21×21 system (38)–(39) is always solvable and results in all C_{ijkl} components oriented in the original coordinate system of C_{ijkl}^{A}. The resultant tensor has, in general, a symmetry different from the input tensors. The symmetry can both increase and decrease, depending on the mutual orientation R, the twinning plane orientation **n**, and the volume fraction λ. Illustrative examples of symmetries of twinned structure in a 2D case are shown in Fig. 3.

From the known effective elastic coefficients, the eigenmodes and eigenfrequencies of a twinned parallelepiped can be evaluated. To do that, we need to determine the orientation of parallelepiped's faces with respect to the coordinate system of the resultant C_{ijkl} tensor. This can be easily done by stating

$$\mathbf{m}=(1-\lambda)\mathbf{m}^{A}+\lambda\mathbf{m}^{\tilde{B}},\tag{41}$$

where $\mathbf{m}^{A}$ is the parallelepiped face normal orientation in variant A and $\mathbf{m}^{\tilde{B}}$ in variant B rotated to A by rotation R. The resultant faces are not exactly planar; they consist of planar facets of two different orientations forming together a rough surface. However, if our assumption of fine structure is satisfied, the surfaces are nearly planar and do not effect the global vibrational properties of the sample.

7.4 Example: RUS analysis of the finely twinned compound structure of CuAlNi

The specimen with the twinned martensitic microstructure was prepared from the CuAlNi crystal (the 3rd section) by a stress-induced transition. The elastic coefficients of a single crystal were known for this material (determined from a single-variant measurement), so the experimentally obtained and evaluated results could be easily compared.

The effective elastic coefficients were inversely determined from the RUS measurement as if the twinned specimen was homogeneous. Then, the elastic coefficients of the single variant were tried do be determined by simplex minimization of the error function

$$\begin{aligned}&F\left(C_k^{\text{single}\atop\text{variant}}\right)\\&=\sum_k\left(C_k^{\text{effective,}\atop\text{experimental}}-C_k^{\text{effective,}\atop\text{evaluated}}\left(C_k^{\text{single}\atop\text{variant}},\lambda\right)\right)^2.\end{aligned}\tag{42}$$

This microstructure consisted of thin *Compound twins* of approximatively 10% vol. of one variant in another. Both opposite surfaces were observed to reveal possible crosstwins structure inside the specimen. Based on the microscopic analysis, we could find that the twined structure fulfils both our conditions on an ideal case of a fine, homogeneously twinned structure, and the volume fracture λ was estimated. The optical micrograph of the examined twinned specimen and a scheme of the Compound twins are shown in Fig. 4a.

In the Compound twins, the two involved variants share a common crystallographic axis (Fig. 4b), and, thus, the twinned structure retains a relatively high symmetry, compared to the more general types of twinning.

Obviously, for $\lambda \in \{0; 0.5; 1\}$, the resulting microstructure is exactly orthorhombic. For any other volume fraction, the resulting symmetry is monoclinic with 13 independent elastic coefficients. In our case of $\lambda = 0.1$, the structure is slightly monoclinic, with the experimentally obtained effective elastic constants

$$C_{ij}^{\text{effective experimental}} = \begin{pmatrix} 191.54 \pm 0.88 & 139.61 \pm 0.65 & 70.54 \pm 1.39 & 0 & -0.33 \pm 0.01 & 0 \\ & 149.25 \pm 0.60 & 97.98 \pm 1.24 & 0 & -0.04 \pm 0.01 & 0 \\ & & 237.79 \pm 1.57 & 0 & 0.37 \pm 0.01 & 0 \\ & & & 63.4 \pm 0.17 & 0 & <0.01 \\ & & & & 24.16 \pm 0.14 & 0 \\ & \text{symm.} & & & & 62.67 \pm 0.28 \end{pmatrix} \text{[GPa]}, \tag{43}$$

which is close to the orthorhombic symmetry of the major variant. The experimental values (43) were determined by the stabilized inversion procedure including RUS and a pulse-echo data obtained on the same twinned sample with the orientation of parallelepiped faces given by (41). Since the monclinicity is negligible, it is convenient to approximate such monoclinic structure by an orthorhombic structure with the symmetry axes parallel to the principal directions of the major variant. This approximation significantly lowers the dimension of the inverse problem for the twinned specimen (from 13 to 9).

Comparison of elastic coefficients of the single variant determined from the single-variant specimen and from the twinned specimen is shown in Table 2. The error ranges are determined as 3σ intervals from 25 calculations for input monoclinic coefficients taken randomly within the accuracy intervals from the experimental matrix (43). The structure orientation was taken as fixed. We can note that this Monte Carlo approach is stable with respect to the experimental uncertainties. The results are in a good agreement with the single-variant measurement (the left column), small discrepancies can be assigned either to the above discussed approximation or to inaccuracy in the input volume fraction. The latter was checked by taking the volume fraction λ as an independent parameter, which was optimized together with the elastic coefficients. However, such extension of the error function (42) did not cause any dramatic changes in the

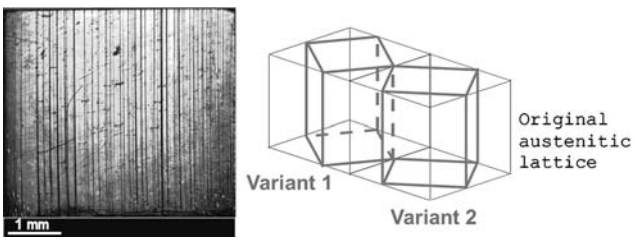

Fig. 4 Optical micrograph of the Compound twinned specimen (*on the left*) and a schematic sketch of the Compound twins (*on the right*)

Table 2 Comparison of elastic coefficients obtained from a single variant, from a twinned specimen with the volume fraction considered as $\lambda = 0.1$, and for optimized volume fraction $\lambda = 0.097$

[GPa]	Measured on a single variant	Determined from a twinned specimen	Optimized volume Fraction (9.7%)
$C_{11}^{\text{single variant}}$	185.3 ± 1.1	186.8 ± 1.1	187.0 ± 1.3
$C_{22}^{\text{single variant}}$	151.3 ± 0.8	153.7 ± 0.8	153.5 ± 0.8
$C_{33}^{\text{single variant}}$	241.9 ± 2.4	243.7 ± 2.1	243.4 ± 2.2
$C_{44}^{\text{single variant}}$	63.2 ± 0.2	64.5 ± 0.8	64.5 ± 0.4
$C_{55}^{\text{single variant}}$	23.9 ± 0.2	23.8 ± 0.8	23.9 ± 0.9
$C_{66}^{\text{single variant}}$	62.0 ± 0.4	61.7 ± 0.5	61.7 ± 0.6
$C_{23}^{\text{single variant}}$	88.0 ± 1.8	91.2 ± 1.6	91.5 ± 1.5
$C_{13}^{\text{single variant}}$	67.8 ± 1.8	65.4 ± 1.4	65.4 ± 1.7
$C_{12}^{\text{single variant}}$	141.8 ± 0.8	142.3 ± 0.7	142.1 ± 0.8

resultant elastic coefficients, as can be seen in the third column of Table 2. The optimal volume fraction was obtained as $\lambda = 0.097$, which is in surprising agreement with the estimation from optical observation.

8 Conclusions

This paper brought an analysis of applicability of the RUS measurements for experimental investigation of elastic properties of ferroelastic single crystals. Due to the strong anisotropy, the effect of some of the elastic coefficients on the measured spectra is suppressed such that these coefficients cannot be reliably determined. For this reason, we introduced a procedure allowing us to separate the reliably determined linear combinations of elastic coefficients from those which cannot be obtained with comparable accuracy. Via this approach, the maximal information obtainable from the RUS measurements can be estimated. Moreover, this approach showed that the RUS technique and the pulse-echo measurements are complementary in the sense that the combinations unobtainable from RUS can be reliably determined from phase velocity measurements in directions of the specimen's face normals, and vice versa.

In the martensitic phase, the ferroelastics can be often found in a form of fine periodic microstructures. The RUS method was shown to be applicable for experimental investigation of such microstructured media and enabled the elastic coefficients of the single variants (single components of the microstructure) to be determined from measurements on the microstructured specimens. That was possible due to known geometric relations between particular variants inside the microstructure, which enabled a simple homogenization of the elastic properties.

Acknowledgements Supports from the Marie-Curie Research Training Network project MULTIMAT (MRTNCT-2004 505226), the project No. 101/06/0768 of the Czech Science Foundation, the institutional project of IT ASCR, v.v.i., CEZ:AV0Z20760514 are greatly acknowledged. The authors wish to express their great thanks to Dr. J. Plešek for a critical reading of the manuscript and helpful comments.

References

1. A. Migliori, J.L. Sarrao, *Resonant Ultrasound Spectroscopy* (Wiley, New York, 1997)
2. P.R. Heyliger, H. Ledbetter, I. Reimanis, J. Acoust. Soc. Am. **114**, 2618 (2003)
3. J.E. Vuorinen, R.B. Schwarz, C. McCullough, J. Acoust. Soc. Am. **108**, 574 (2000)
4. P.R. Heyliger, J. Acoust. Soc. Am. **107**, 1235 (2000)
5. L. Ostrovsky, A. Lebedev, A. Matveyev, A. Potapov, A. Sutin, I. Soustova, P. Johnson, J. Acoust. Soc. Am. **110**, 1770 (2001)
6. R.G. Leisure, K. Foster, J.E. Hightower, D.S. Agosta, Math. Sci. Eng. A **370**, 34 (2004)
7. S. Petit, Ultrasonics **43**, 802 (2005)
8. K.E.-A. Van Den Abeele, P.A. Johnson, A. Sutin, Res. Nondestruct. Eval. **12**, 17 (2000)
9. K.E.-A. Van Den Abeele, J. Acoust. Soc. Am. **122**, 73 (2007)
10. H. Ogi, K. Sato, T. Asada, M. Hirao, J. Acoust. Soc. Am. **112**, 2553 (2002)
11. P. Sedlák, H. Seiner, M. Landa, V. Novák, P. Šittner, L. Mañosa, Acta Mater. **53**, 3643 (2005)
12. M. Landa, V. Novák, P. Sedlák, L. Mañosa, P. Šittner, Material Science Forum. Trans. Tech. Publ. 351 (2005)
13. H. Seiner, P. Sedlák, M. Landa, in *Proceedings of 2006 IEEE International Ultrasonics Symposium*, October 3–6, 2006, Vancouver (Canada), CD-ROM
14. M. Landa, P. Sedlák, H. Seiner, L. Bicanová, P. Šittner, V. Novák, in *Proceedings of International Congress on Ultrasonics*, April 9–12, 2007, Vienna (Austria), CD-ROM (http://www.icultrasonics.org/)
15. H.H. Demarest Jr., J. Acoust. Soc. Am. **49**, 768 (1971)
16. W.M. Visscher, A. Migliori, T.M. Bell, R.A. Reinert, J. Acoust. Soc. Am. **90**, 2154 (1991)
17. I. Ohno, J. Phys. Earth **24**, 355 (1976)